




Cite this: *RSC Adv.*, 2021, 11, 1

A simple colorimetric and ratiometric fluoride ion probe with large color change†

Heng Shi, Hongjin Chen, Xiangguo Li, Jieni Xing, Gang Zhang,  Rui Zhang and Jian Liu *

Two colorimetric and ratiometric fluoride ion probes **SHJ-1** and **SHJ-2** based on the acylhydrazone skeleton have been developed. Among the eight anions (F^- , Cl^- , Br^- , I^- , ClO_4^- , $H_2PO_4^-$, HSO_4^- , CH_3COO^-), the present probes showed high selectivity and sensitivity toward fluoride ion detection with obvious color change. Notably, the probe **SHJ-1** exhibited a red shift of 145 nm upon fluoride sensing, which is the largest value among fluoride ion probes based on acylhydrazone derivatives to date. 1H NMR titration study and theoretical calculations suggested that the strong binding of the probe **SHJ-1** to fluoride as well as the further deprotonation may facilitate the intramolecular charge transfer transition. These two probes are 1 : 1 complexed with fluoride ions, and the detection limits were calculated to be $1.24 \mu M$ for **SHJ-1** and $15.73 \mu M$ for **SHJ-2**.

Received 6th August 2020
Accepted 13th December 2020

DOI: 10.1039/d0ra06782b

rsc.li/rsc-advances

1. Introduction

The sensing and recognition of anions have been considered as a hot topic due to the fundamental and crucial roles of anions in the environment and biological fields.^{1–10} Among them, fluoride is an essential trace element in the human body and widely exists in nature in the form of fluorine ions.^{11–15} Either deficiency or excess of fluoride in the human body would lead to dental caries, such as osteoporosis, fluorosis and urolithiasis, and so on.^{16–18} In this regard, the detection of fluoride ions has received great attention, and tremendous effort has been devoted to the development of chemical probes for fluoride ions toward high selectivity, good sensitivity and rapid response.^{19–22} The concept of molecular engineering of fluoride ion probes was highly dependent on its unusual chemical properties involving small ionic radius,^{23–25} high charge density and hard Lewis basic nature.²⁶ So far, the recognition mechanisms involving B–F complexation,²⁷ F^- -induced deprotonation through H-bonding,^{28–32} F^- -mediated desilylation of Si–O/Si–C bonds,^{33–37} and intramolecular charge transfer have been demonstrated.³⁸ For naked-eye detection, it is significant to design chemical probes with large color change toward fluoride ion sensing.³⁹

Recently, fluoride ion probes based on acylhydrazone derivatives have been successfully developed for naked-eyes detection,^{40,41} mainly originated from the strong binding between

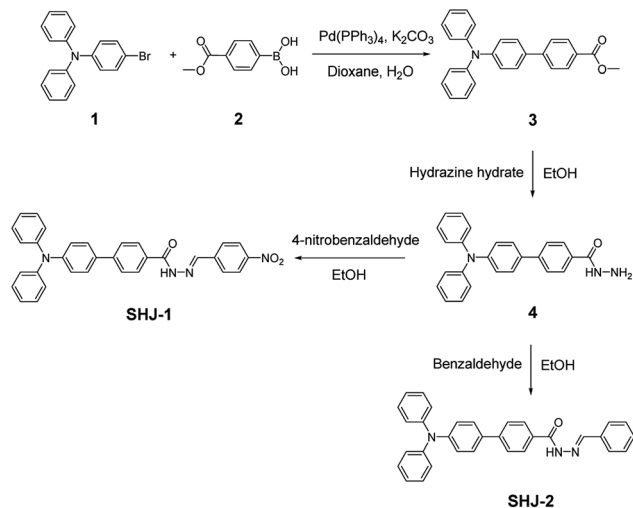
active proton in acylhydrazone moiety and F^- , which further induced the deprotonation of the probe and facilitate the $\pi-\pi^*$ transition in low energy,⁴² resulting in a red shift of absorption spectra.⁴³ The reported fluoride ion probes based on acylhydrazone derivatives were normally constructed by introducing a non-conjugated acylhydrazone unit among two conjugated moieties.⁴⁴ The increase of conjugation length of the probes up on fluoride sensing normally lead to a moderate red shift.⁴⁵ Therefore, the development of acylhydrazone-based fluoride probes with large red shift was still a challenge. Acylhydrazones are normally prepared by condensation reactions between acylhydrazines and aldehydes. Thus it is easy to install an electron donating group and an electron withdrawing group on both sides of the acylhydrazone moiety, establishing an acylhydrazone with a non-conjugated donor-acceptor (D–A) configuration. It can be anticipated that the F^- -induced deprotonation of this type molecules through H-bonding may facilitate the keto–enol tautomerism of the acylhydrazone group as well as the intramolecular charge transfer transition, resulting in large red shift in absorption spectra and large color change toward fluoride ion sensing.

Based on this assumption, herein, we designed a new fluoride probe **SHJ-1** by introducing a nonconjugated acylhydrazone unit between a triphenylamine-based electron donor and a nitrobenzene-based electron acceptor (Scheme 1). We also prepared an analogue **SHJ-2** by using benzene group instead of nitrobenzene in **SHJ-1**. The probe **SHJ-1** with an unique configuration exhibited a distinct color change from undertint to dark red up on fluoride sensing, being originated from a red-shift up to 145 nm in the adsorption spectra, which was superior to its analogue **SHJ-2** with a red shift around 78 nm.

Jiangsu Co-Innovation Center of Efficient Processing and Utilization of Forest Resources, Jiangsu Key Lab of Biomass-based Green Fuels and Chemicals, College of Chemical Engineering, Nanjing Forestry University, Nanjing 210037, China. E-mail: liu.jian@njfu.edu.cn

† Electronic supplementary information (ESI) available: Spectra characterization, DFT calculation. See DOI: 10.1039/d0ra06782b





Scheme 1 Synthetic route of SHJ-1 and SHJ-2.

2. Experimental section

The synthetic route of **SHJ-1** and **SHJ-2** was shown in Scheme 1. The target probes **SHJ-1** and **SHJ-2** were prepared by condensation reactions from a same intermediate **4**, which was synthesized by hydrazinolysis of the ester **3**. The ester **3** was prepared *via* Suzuki coupling between compounds **1** and **2**. The ¹H- and ¹³C-NMR measurements were performed by a DRX-600 spectrometer (Bruker BioSpin) at room temperature using CDCl₃ or DMSO-*d*₆ as a solvent and tetramethylsilane as an internal standard. FT-IR spectra were recorded using KBr pellets by a PerkinElmer Spectrum Two FT-IR spectrometer. Elemental analyses were performed by PE 2400 II Elemental Analyzer. High resolution mass of **SHJ-1** and **SHJ-2** was characterized by matrix-assisted laser desorption/ionization time of flight mass spectrometry (MALDI-TOF MS) using UltrafleXtreme TOF/TOF (Bruker). UV-vis absorption spectra were measured in THF solution using UV-3600 Spectrophotometer (SHIMADZU), respectively.

Preparation of compound 3

Compound **1** (500 mg, 1.550 mmol) and **2** (278 mg, 1.550 mmol) were added to a two-necked flask (50 mL), followed by potassium carbonate (750 mg, 5.425 mmol), tetrakis(triphenylphosphine)palladium (180 mg, 0.155 mmol), 1,4-dioxane (26 mL) and water (3 mL), the mixture was stirred at 90 °C for 12 hours under N₂ atmosphere. After the reaction was completed, the solution was cooled to room temperature, the solvent was distilled off under reduced pressure, water was added, extracted with dichloromethane, the organic phase was collected and dried over anhydrous sodium sulfate. After drying, the solvent was removed by vacuum distillation and purified by column chromatography with PE/EA (30/1, v/v) as an eluent to afford compound **4** (420 mg, yield: 72%). ¹H NMR (CDCl₃, 600 MHz, δ, ppm): 8.09 (d, *J* = 8.4 Hz, 2H), 7.64 (d, *J* = 8.4 Hz, 2H), 7.51 (d, *J* = 8.4 Hz, 2H), 7.30–7.26 (m, 4H), 7.15 (d, *J* = 7.8 Hz, 6H) 7.06 (t, *J*₁ = 7.2 Hz, *J*₂ = 7.2 Hz, 2H), 3.94 (s, 3H)

(Fig. S1†). ¹³C NMR (CDCl₃, 150 MHz, δ, ppm): 167.2, 148.2, 147.6, 145.2, 133.5, 130.2, 129.5, 128.4, 128.1, 126.5, 124.9, 124.8, 123.5, 123.4, 52.2 (Fig. S2†). Anal. calcd for C₂₆H₂₁NO₂: C, 82.30; H, 5.58; N, 3.69. Found: C, 82.23; H, 5.62; N, 3.64.

Preparation of compound 4

Compound **3** (76 mg, 0.200 mmol), hydrazine hydrate (0.1 mL) and absolute ethanol (5 mL) were added to a two-necked bottle of 25 mL, filled with nitrogen to protect, heated to reflux, and reacted for 24 hours under stirring. After the reaction was completed, the solution was cooled to room temperature, the solvent was distilled off under reduced pressure, water was added, extracted with dichloromethane, the organic phase was collected and dried over anhydrous sodium sulfate. After drying, the solvent was removed by vacuum distillation and purified by column chromatography with PE/EA (2/1, v/v) as an eluent to afford compound **4** (47 mg, yield: 62%). ¹H NMR (CDCl₃, 600 MHz, δ, ppm): 9.36 (s, 1H), 8.27 (d, *J* = 13.2 Hz, 2H), 7.93 (s, 2H), 7.70–7.68 (d, *J* = 12.6 Hz, 2H), 7.51 (d, *J* = 12.6 Hz, 2H), 7.31–7.26 (m, 4H), 7.15 (m, 6H), 7.07 (m, 2H) (Fig. S3†). ¹³C NMR (CDCl₃, 150 MHz, δ, ppm): 148.1, 147.6, 144.3, 136.5, 133.3, 130.6, 129.5, 127.9, 127.6, 126.8, 124.8, 123.5, 123.4 (Fig. S4†). Anal. calcd for C₂₅H₂₁N₃O: C, 79.13; H, 5.58; N, 11.07. Found: C, 79.07; H, 5.63; N, 11.03.

Preparation of SHJ-1

Compound **4** (35 mg, 0.092 mmol) and *p*-nitrobenzaldehyde (55 mg, 0.368 mmol) were added to a two-necked flask of 25 mL, and then 5 mL absolute ethanol was added, the mixture was stirred at 80 °C for 12 hours under N₂ atmosphere. After the reaction was completed, the solution was cooled to room temperature, the solvent was distilled off under reduced pressure, water was added, extracted with dichloromethane, the organic phase was collected and dried over anhydrous sodium sulfate. After drying, the solvent was removed by vacuum distillation and purified by column chromatography with PE/EA (3/1, v/v) as an eluent to afford probe **SHJ-1** (42 mg, yield: 89%). ¹H NMR (DMSO-*d*₆, 600 MHz, δ, ppm): 12.19 (s, 1H), 8.56 (s, 1H), 8.30 (s, 2H), 8.00 (s, 4H), 7.81 (s, 2H), 7.69 (m, 2H), 7.34 (s, 4H), 7.07 (m, 8H) (Fig. S5†). ¹³C NMR (DMSO-*d*₆, 150 MHz, δ, ppm): 157.4, 148.3, 148.0, 147.3, 145.6, 141.2, 130.1, 128.9, 128.5, 128.4, 126.5, 124.9, 124.6, 124.0, 123.3 (Fig. S6†). MALDI-TOF MS: exact *m/z* calculated for [C₃₂H₂₄N₄O₃]⁺: 512.1848; found: 512.3679 (Fig. S7†). FT-IR (KBr, cm⁻¹): C=O: 1645 cm⁻¹, N-H: 3452 cm⁻¹, -NO₂: 1275 cm⁻¹ (Fig. S8†).

Preparation of SHJ-2

Compound **4** (35 mg, 0.092 mmol) and benzaldehyde (0.1 mL) were added to a two-necked flask of 25 mL, and then 5 mL absolute ethanol was added, the mixture was stirred at 80 °C for 12 hours under N₂ atmosphere. After the reaction was completed, the solution was cooled to room temperature, the solvent was distilled off under reduced pressure, water was added, extracted with dichloromethane, the organic phase was collected and dried over anhydrous sodium sulfate. After drying, the solvent was removed by vacuum distillation and



purified by column chromatography with PE/EA (3/1, v/v) as an eluent to afford probe **SHJ-2** (39 mg, yield: 91%). ^1H NMR (DMSO- d_6 , 600 MHz, δ , ppm): 11.88 (s, 1H), 8.49 (s, 1H), 8.00–7.99 (d, $J = 8.4$ Hz, 2H), 7.81–7.79 (d, $J = 8.4$ Hz, 2H), 7.74 (d, $J = 6.6$ Hz, 2H), 7.70–7.69 (d, $J = 9.0$ Hz, 2H), 7.45 (m, 2H), 7.34 (t, $J_1 = 7.8$ Hz, $J_2 = 8.4$ Hz, 4H), 7.11–7.05 (m, 9H) (Fig. S9 †). ^{13}C NMR (DMSO- d_6 , 150 MHz, δ , ppm): 163.2, 148.0, 147.7, 147.1, 142.9, 134.5, 132.6, 131.6, 130.4, 129.9, 129.1, 128.5, 128.1, 127.3, 126.2, 124.6, 123.8, 123.0 (Fig. S10 †). MALDI-TOF MS: exact m/z calculated for $[\text{C}_{32}\text{H}_{25}\text{N}_3\text{O}]^+$: 467.1998; found: 467.3378 (Fig. S11 †). FT-IR (KBr, cm^{-1}): C=O: 1652 cm^{-1} , N-H: 3442 cm^{-1} (Fig. S12 †).

3. Results and discussion

Firstly, we investigated the naked eye sensing of probes **SHJ-1** and **SHJ-2** toward various anions (F^- , Cl^- , Br^- , I^- , ClO_4^- , H_2PO_4^- , HSO_4^- , AcO^-) by adding 6 and 23.33 equiv. tetrabutylammonium salts in DMSO solutions, respectively. As shown in Fig. 1, obvious color changes were observed from undertint to dark red for the probe **SHJ-1** and from undertint to light yellow for **SHJ-2** after the addition of fluoride ion salt, respectively. However, after being treated with other seven anions, almost no color variance was observed in the solution of probes in DMSO. The results suggested that the present two probes performed

naked-eye sensitivity and good selectivity for fluoride ion detection. The absorption spectra monitoring results indicated that the maximum absorption peak of **SHJ-2** showing a red shift of 25 nm up on the addition of fluoride ion salt. Interestingly, a large red shift of 145 nm was recorded for **SHJ-1** during the fluoride sensing process, which resulted in a more distinct color change. It is noted that it is the largest value of bathochromic shift among the reported fluoride probe based on acylhydrazone derivatives up to date (Table S1 †). Moreover, probes **SHJ-1** and **SHJ-2** exhibited good stability in DMSO and transient responding toward fluoride ions detection (Fig. S13 and S14 †).

UV-vis absorption titration test was performed to study the influence of adding amount of fluoride ion on the absorption spectra of two probes **SHJ-1** and **SHJ-2**, respectively. As shown in Fig. 2a, with the adding amount of fluoride ion increasing, it could be clearly found that a new absorption peak around 500 nm for **SHJ-1** appeared and increased in intensity gradually, while the intensity of the maximum absorbance peaks of the pristine probe in the UV region around 355 nm decreased. The large red shift upon F^- sensing resulted in a distinct color change from undertint to dark red. When 10 equiv. of F^- was added, the intensity the peak at 500 nm reached a maximum value, which implied that the mixture formed by **SHJ-1** and fluoride ions reached a saturation value. The well-positioned isosbestic point was observed at 411 nm, suggesting the existence of a well-described binding equilibrium in the solution of **SHJ-1** with the addition of TBAF. Moreover, a linear relationship

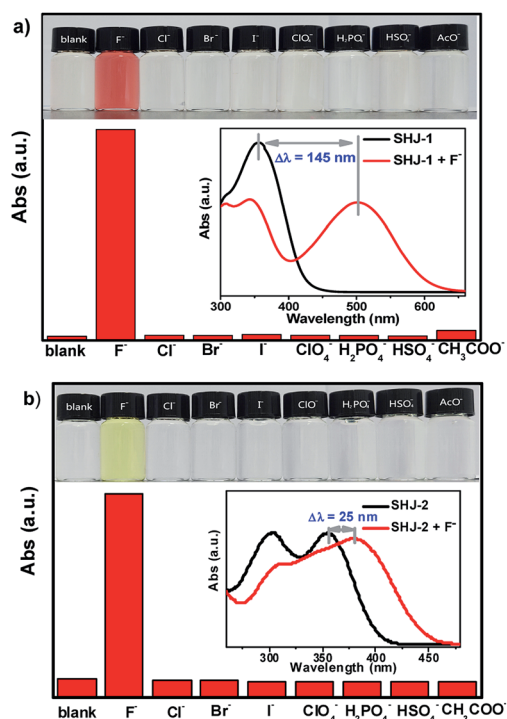


Fig. 1 The intensity of the maximum visible absorption peak of probes **SHJ-1** (a) and **SHJ-2** (b) with the addition of 6 and 23.33 equiv. of various anions (as tetrabutylammonium salt) in DMSO solution at room temperature, respectively (inset: color changes of probes with the addition of 6 and 23.33 equiv. of various anions under ambient light, respectively, and the corresponding variation of the UV-vis absorption spectra toward F^- sensing).

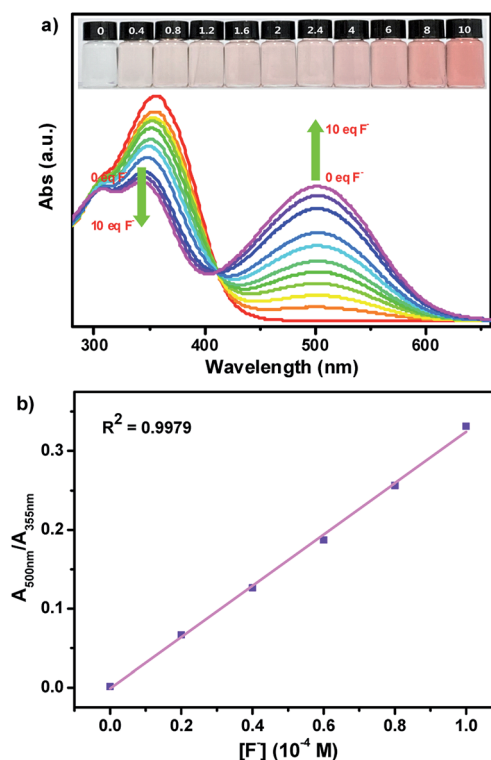


Fig. 2 (a) Absorption spectra of probe **SHJ-1** in DMSO with the addition of different equiv. of TBAF (inset: color changes of probes with the addition of different equiv. of F^- under ambient light); (b) the absorbance ratio ($A_{500\text{ nm}}/A_{355\text{ nm}}$) of **SHJ-1** versus F^- concentrations.

between the absorbance ($A_{500\text{ nm}}/A_{355\text{ nm}}$) of **SHJ-1** and the concentration of TBAF was given by a ratiometric absorption process for the quantitative detection of F^- , which demonstrated that **SHJ-1** can be described as a ratiometric probe (Fig. 2b). On the other hand, upon the addition of fluoride ion, the intensity of absorption peak of **SHJ-2** at 355 nm decreased while a new absorption band at 380 nm appeared and its intensity was increased gradually, which resulted in a color change from colorless to light yellow attributed to the red shift of 25 nm. The systematic titration analysis results implied that **SHJ-2** was also a ratiometric probe for F^- detection with an isosbestic point at 365 nm (Fig. S15†). The probable reason for the observed distinction of red shift value between **SHJ-1** and **SHJ-2** toward F^- sensing will be discussed *vide infra*.

In order to further investigate the stoichiometric ratio of two probes **SHJ-1** and **SHJ-2** with fluoride ion, we conducted a Job's plot experiment in their DMSO solutions. As shown in Fig. 3a, the intensity of the absorption band reached the maximum

when the value of $[\text{F}^-]/([\text{F}^-] + [\text{SHJ-1}])$ is 0.5, suggesting the formation of an 1 : 1 stoichiometric complex of **SHJ-1** and fluoride ions. This result was further confirmed by the Benesi-Hildebrand plot of $1/(A - A_0)$ at 500 nm against $[\text{F}^-]^{-1}$, with a good linear relationship ($R^2 = 0.9983$) (Fig. 3b). The similar systematical analysis for the probe **SHJ-2** implied that it exhibited similar complexing behavior (Fig. S16†). In addition, the association constants (K_a) between these two probes and F^- were calculated to be $1.9 \times 10^3\text{ M}^{-1}$ for **SHJ-1** and $0.3 \times 10^3\text{ M}^{-1}$ for **SHJ-2**, respectively. The result implied that **SHJ-1** has more binding affinity for F^- than that of **SHJ-2**. Moreover, the limit of detection (LOD) of these two probes were calculated according to the equation $\text{LOD} = 3\sigma/K$ (where σ was the standard deviation of 15 blank measurements, and K was the slope obtained from the graph of absorbance vs. the concentration of TBAF). As shown in Fig. 3c and S16c,† the limits of detection of these two probes were calculated to be $1.24\text{ }\mu\text{M}$ for **SHJ-1** and $15.73\text{ }\mu\text{M}$ for **SHJ-2**, respectively. The results further indicated that the superior performance of **SHJ-1** in comparison with that of **SHJ-2** for fluoride ion detection.

We also investigated the impact of the water content in the medium on the sensing effect of these probes. As shown in Fig. 4, with increasing the water content in DMSO, the absorption intensity in the visible region of probe **SHJ-1** in the presence of 10 equiv. TBAF decreased gradually. When the water content reach up to 5%, the absorption band around 480 nm disappeared, and the sample become undertint. A similar phenomenon was observed in the sample of **SHJ-2** (Fig. S17†). The results implied that the present two probes are not effective for the fluoride ion detection under high water content. Moreover, we study the solvent compatibility for the probe **SHJ-1** toward fluoride ion sensing. As a result, the probe **SHJ-1** can also achieve naked-eyes detection of fluoride ion in DMF and DCM (Fig. S18†).

The interaction between fluoride ion and the present probes were investigated by monitoring the ^1H NMR spectra of probe **SHJ-1** in $\text{DMSO}-d_6$ with the addition of tetrabutylammonium fluoride. As shown in Fig. 5, a signal peak around 12.19 ppm that attributed to the proton in $-\text{NH}$ group was observed in the

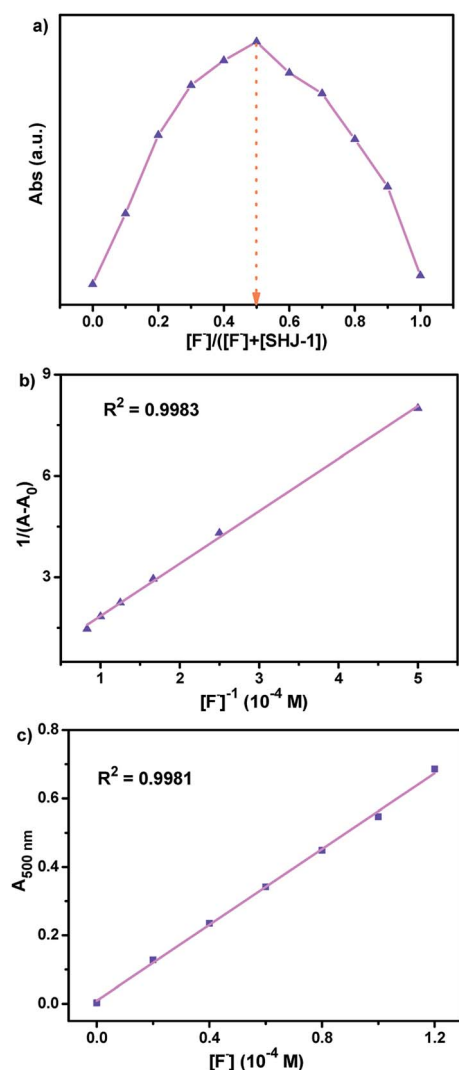


Fig. 3 (a) Job's plot for complexation of **SHJ-1** with F^- ; (b) Benesi-Hildebrand plot of **SHJ-1** with F^- ; (c) absorbance of **SHJ-1** in the presence of TBAF at different concentration in DMSO.

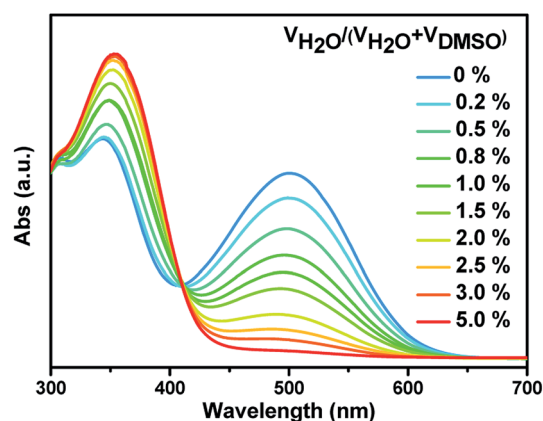


Fig. 4 Absorbance spectra of probe **SHJ-1** in the presence of 2 equiv. TBAF in THF with various content of water.



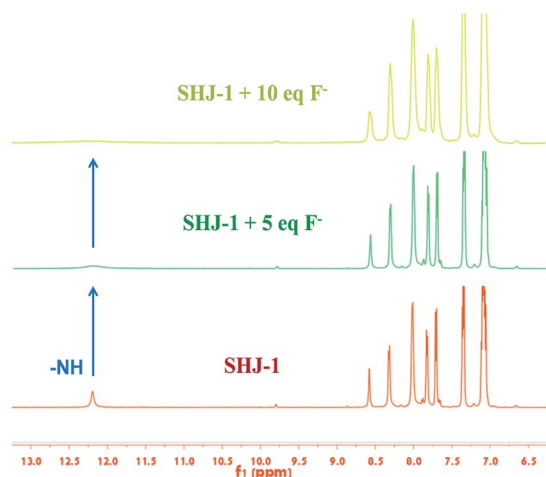


Fig. 5 ^1H NMR titration spectra of the probe **SHJ-1** in $\text{DMSO}-d_6$ in presence of different equivalents of TBAF.

pristine **SHJ-1**. With the addition of 5 equiv. of TBAF, the intensity of this peak corresponding to $-\text{NH}$ group was decreased obviously. When 10 equiv. of TBAF was added into the sample, the resonance signal of the active proton in $-\text{NH}$ group disappeared, which revealed that the probe **SHJ-1** may undergo a deprotonation process during the fluoride ions sensing. The result was similar with those of fluoride ion probes based on acylhydrazone skeleton reported previously.^{40–45}

To gain further insight into the observed difference of red shift value of the absorption band between **SHJ-1** and **SHJ-2** during the fluoride ion sensing, the optimized geometries for probes and probes with F^- were optimized by DFT calculation using Gaussian 16, respectively. As shown in Fig. 6 and S19,[†] the probe **SHJ-1** and **SHJ-2** bonded F^- at the N–H position of acylhydrazone group, respectively. For the probe **SHJ-1**, the N–H bond was become elongate obviously from 1.016 Å to 1.422 Å after being captured by F^- , and the distance between F^- and active proton was 1.047 Å. Moreover, the angle of the N–N–C in the acylhydrazone moiety also decreased from 120.9° to 113.4° after bonding with F^- . These results implied that the H–F strong interactions may lead to the deprotonation of the probe

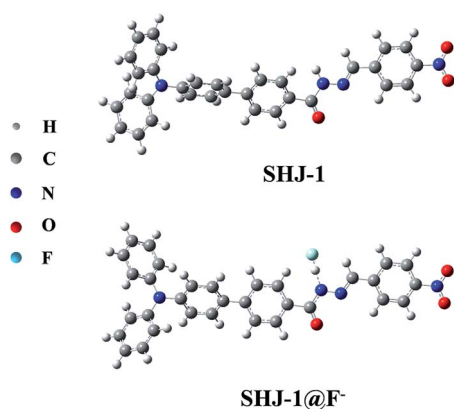


Fig. 6 Optimized structures of **SHJ-1** and **SHJ-1@F⁻**.

SHJ-1, and the lone pair electrons in nitrogen atom may facilitate the keto–enol tautomerism of the acylhydrazone moiety, which resulted in the π -conjugate throughout the molecular backbone. Interestingly, due to the additional electron-withdrawing group ($-\text{NO}_2$) in **SHJ-1**, the deprotonation may cause a donor– π -acceptor configuration and a new absorption band attributed to the intramolecular charge transfer transition. As a result, a red shift up to 145 nm was observed in the case of **SHJ-1** toward fluoride ion sensing.

4. Conclusion

In summary, we have developed a new strategy for the molecular engineering of fluoride ion probes toward large color change. The present probes exhibited naked-eyes detection for fluoride ion, with a color change from undertint to dark red for **SHJ-1** and from undertint to light yellow for **SHJ-2**. ^1H NMR titration study and DFT calculations suggested that the H–F strong interactions as well as further deprotonation of the **SHJ-1** may facilitate the keto–enol tautomerism of the acylhydrazone moiety and intramolecular charge transfer transition from triphenylamine donor part to nitrobenzene-based electron acceptor. As a result, **SHJ-1** exhibited a large red shift up to 145 nm toward fluoride ion sensing, as well as a low detection limit around 1 μM . The present strategy are expected to be employed for the development of other ion probes based on deprotonation mechanism.

Conflicts of interest

The authors declare that they have no conflict of interest.

Acknowledgements

This work was supported in part by the Natural Science Foundation of Jiangsu Province (BK20191385), the High Level Talent Project of Nanjing Forestry University (GXL2018003) and the National Natural Science Foundation of China (21631006).

Notes and references

- 1 A. Tigreros and J. Portilla, *RSC Adv.*, 2020, **10**, 19693–19712.
- 2 L. Wang, H. Ding, X. Ran, H. Tang and D. Cao, *Dyes Pigm.*, 2020, **172**, 107857.
- 3 D. Udhayakumari, *Spectrochim. Acta, Part A*, 2020, **228**, 117817.
- 4 R. Ali, R. C. Gupta, S. K. Dwivedi and A. Misra, *New J. Chem.*, 2018, **42**, 11746–11754.
- 5 X. Pang, J. Ge, X. Yu, Y. Li, F. Shen, Y. Wang and J. Ren, *New J. Chem.*, 2019, **43**, 10554–10559.
- 6 S. Yang, Y. Liu and G. Feng, *RSC Adv.*, 2013, **3**, 20171–20178.
- 7 R. Wang, X. Shu, Y. Fan, S. Li, Y. Jin and C. Huang, *RSC Adv.*, 2018, **8**, 39394–39407.
- 8 J. Li, H. Lin, Z. Cai and H. Lin, *Spectrochim. Acta, Part A*, 2009, **72**, 1062–1065.
- 9 X. Yang, G. Zhang, Y. Li, Z. Liu, X. Gong, B. Gao, G. Zhang, Y. Cui and G. Sun, *RSC Adv.*, 2015, **5**, 22455–22462.



- 10 S. N. Sahu, S. K. Padhan and P. K. Sahu, *RSC Adv.*, 2016, **6**, 90322–90330.
- 11 S. Dhiman, M. Ahmad, N. Singla, G. Kumar, P. Singh, V. Luxami, N. Kaur and S. Kumar, *Coord. Chem. Rev.*, 2020, **405**, 213138.
- 12 J. Han, J. Zhang, M. Gao, H. Hao and X. Xu, *Dyes Pigm.*, 2019, **162**, 412–439.
- 13 Y.-H. Zhao, Y. Li, Y. Long, Z. Zhou, Z. Tang, K. Deng and S. Zhang, *Tetrahedron Lett.*, 2017, **58**, 1351–1355.
- 14 G. Zhang, L. Wang, X. Cai, L. Zhang, J. Yu and A. Wang, *Dyes Pigm.*, 2013, **98**, 232–237.
- 15 J. Shi, W. Shu, Y. Wu, J. Jing, R. Zhang and X. Zhang, *Anal. Methods*, 2019, **11**, 3844–3850.
- 16 A. R. Chowdhury, P. Ghosh, B. G. Roy, S. K. Mukhopadhyay, P. Mitra and P. Banerjee, *RSC Adv.*, 2015, **5**, 62017–62023.
- 17 S. N. Sahu, S. K. Padhan and P. K. Sahu, *RSC Adv.*, 2016, **6**, 90322–90330.
- 18 Y. Feng, X. Li, H. Ma, Z. Zhang, M. Zhang and S. Hao, *Dyes Pigm.*, 2018, **153**, 200–205.
- 19 W.-J. Qu, J. Guan, T.-B. Wei, G.-T. Yan, Q. Lin and Y.-M. Zhang, *RSC Adv.*, 2016, **6**, 35804–35808.
- 20 C. Saravanan, S. Easwaramoorthi, C. Y. Hsiow, K. Wang, M. Hayashi and L. Wang, *Org. Lett.*, 2014, **16**, 354–357.
- 21 Y. Yin, T. Sarma, F. Wang, N. Yuan, Z. Duan, J. L. Sessler and Z. Zhang, *Org. Lett.*, 2019, **21**, 1849–1852.
- 22 F. S. Zabihi and A. Mohammadi, *Spectrochim. Acta, Part A*, 2020, **238**, 118439.
- 23 G. Turkoglu, *New J. Chem.*, 2020, **44**, 9485–9492.
- 24 M. Du, B. Huo, M. Li, A. Shen, X. Bai, Y. Lai, J. Liu and Y. Yang, *RSC Adv.*, 2018, **8**, 32497–32505.
- 25 Y. Zhang, Y. Deng, N. Ji, J. Zhang, C. Fan, T. Ding, Z. Cao, Y. Li and Y. Fang, *Dyes Pigm.*, 2019, **166**, 473–479.
- 26 S. K. Asthana, A. Kumar, Neeraj and K. K. Upadhyay, *Tetrahedron Lett.*, 2014, **55**, 5988–5992.
- 27 T. Tao, J. Zhao, H. Chen, S. Mao, J. Yu and W. Huang, *Dyes Pigm.*, 2019, **170**, 107638.
- 28 S. Swami, D. Behera, A. Agarwala, V. P. Verma and R. Shrivastava, *New J. Chem.*, 2018, **42**, 10317–10326.
- 29 W. Lu, M. Zhang, K. Liu, B. Fan, Z. Xia and L. Jiang, *Sens. Actuators, B*, 2011, **160**, 1005–1010.
- 30 L. Zhang, F. Zhang, L. Ding and J. Gao, *Spectrochim. Acta, Part A*, 2020, **237**, 118395.
- 31 Y. Qu, J. Hua and H. Tian, *Org. Lett.*, 2010, **12**, 3320–3323.
- 32 Q. Lin, X. Zhu, Y. P. Fu, Y. M. Zhang, R. Fang, L. Z. Yang and T. B. Wei, *Soft Matter*, 2014, **10**, 5715–5723.
- 33 S. Goswami, A. K. Das, A. Manna, A. K. Maity, H.-K. Fun, C. K. Quah and P. Saha, *Tetrahedron Lett.*, 2014, **55**, 2633–2638.
- 34 X. Yu, L. Yang, T. Zhao, R. Zhang, L. Yang, C. Jiang, J. Zhao, B. Liu and Z. Zhang, *RSC Adv.*, 2017, **7**, 53379–53384.
- 35 Y. Zhou, M.-M. Liu, J.-Y. Li, M.-A. Ye and C. Yao, *Dyes Pigm.*, 2018, **158**, 277–284.
- 36 Y. Yu and C. Dong, *Anal. Methods*, 2015, **7**, 9604–9608.
- 37 B. Qiu, Y. Zeng, L. Cao, R. Hu, X. Zhang, T. Yu, J. Chen, G. Yang and Y. Li, *RSC Adv.*, 2016, **6**, 49158–49163.
- 38 J. Ji, Z. Zhang, F. Zhan, Q. Wang and G. Zheng, *J. Photochem. Photobiol., A*, 2020, **390**, 112349.
- 39 D. Li and Z. Tian, *J. Mol. Struct.*, 2020, **1206**, 127631.
- 40 Y. Chen, B. Bai, Q. Chai, M. Zhang, J. Wei, H. Wang and M. Li, *Soft Matter*, 2019, **15**, 6690–6695.
- 41 H. Shi, F. Zhao, X. Chen, S. Yang, J. Xing, H. Chen, R. Zhang and J. Liu, *Tetrahedron Lett.*, 2019, **60**, 151330.
- 42 J. Jose, A. Sreekanth, A. M. John, S. M. Basheer and P. B. Sreeja, *Res. Chem. Intermed.*, 2018, **45**, 425–435.
- 43 S. Vishwakarma, A. Kumar, A. Pandey and K. K. Upadhyay, *Spectrochim. Acta, Part A*, 2017, **170**, 191–197.
- 44 X. Yuan, X. Xu, C. Zhao, F. Zhang, Y. Lu, Y. Shen and C. Wang, *Sens. Actuators, B*, 2017, **253**, 1096–1105.
- 45 P. Rajamalli and E. Prasad, *Org. Lett.*, 2011, **13**, 3714–3717.

